Fuel 386 (2025) 134341

Contents lists available at ScienceDirect

Fuel

journal homepage: www.elsevier.com/locate/fuel

Full Length Article

Competitive adsorption characteristics of CH_4/O_2 on coal surfaces: Insights at the molecular scale

Chengyang Peng [a], Shujing He [a], Jianhong Kang [a,b,*], Ran Zhang [a], Shasha Si [a], Yiqian Zhou [c]

[a] School of Safety Engineering, China University of Mining and Technology, Xuzhou 221116, China
[b] Key Laboratory of Gas and Fire Control for Coal Mines, China University of Mining and Technology, Xuzhou 221116, China
[c] School of Mathematics and Statistics, Central South University, Changsha 410083, China

ARTICLE INFO

Keywords:
Coal
CH_4/O_2
Competitive adsorption
Adsorption heat
Binding energy

ABSTRACT

Understanding the competitive adsorption characteristics of CH_4 and O_2 on residual coal in underground mine goafs is crucial for elucidating the mechanisms of coal spontaneous combustion. In this study, grand canonical Monte Carlo simulations, molecular dynamics, and density functional theory were employed to investigate the thermodynamic behaviors of CH_4/O_2 competitive adsorption under varying conditions. The adsorption quantities, selectivity, heat, and density distribution of the adsorbed phase were systematically analyzed. Key competitive adsorption sites were identified based on initial adsorption potential, atomic radial distribution, and the binding energy at functional groups. The results revealed that the competitive adsorption of CH_4 and O_2 on coal follows Type I adsorption isotherm characteristics, the adsorption capacity of CH_4 is at least 2.41 times greater than that of O_2 under identical conditions. The selectivity of coal for CH_4 over O_2 was found to decrease exponentially with increasing equilibrium pressure and linearly with rising temperature and CH_4 fraction. At the critical ratio of CH_4:O_2 = 2.15:7.85, the competitive adsorption capacities of CH_4 and O_2 on the coal surface are equivalent, and this equilibrium remains unaffected by variations in pressure or temperature. The potential energy between CH_4 and coal was observed to be stronger than that of O_2. As the CH_4 proportion increases from 0.2 to 0.8, the IAP of CH_4 improves by 8.8 %, while the IAP of O_2 decreases by 14.5 %. From the perspective of adsorption heat, the isosteric heat of O_2 adsorption increased with the CH_4 fraction. The AH of CH_4 decreases by 6.8 %, and that of O_2 decreases by 7.4 % as the temperature rises from 273 K to 413 K and the pressure increases from 0.02 MPa to 2 MPa. Specific adsorption sites for CH_4 and O_2 on coal were primarily located at O and N atoms, while C and H atoms exhibited similar adsorption characteristics. The binding energy of O_2 with oxygen-containing functional groups exceeded its isosteric heat of adsorption, indicating that these functional groups could mitigate the disadvantage of O_2 in competitive adsorption. These findings clarify CH_4/O_2 interactions on coal and provide valuable insights for managing spontaneous combustion risks in goafs.

1. Introduction

Coal Spontaneous Combustion (CSC) is a prevalent hazard in coal mines [2], particularly in leading coal-producing nations such as China, the US, and Australia. [22,32,34,40]. In China, SCC annually results in the loss of over 10 million tons of coal and economic damages surpassing 20 billion yuan [36]. It is also prone to cause secondary disasters such as dust explosions and gas explosions, causing significant human casualties [7,21,24–25]. From 2001 to 2023, there have been 16 major disasters caused by SCC in China, resulting in 353 deaths [24]. A total of 25 underground coal mine fires caused by SCC were recorded in the US during the period 1990–2006 [28]. In 2014, a SCC incident at Turkey's Soma coal mine led to a methane flare-up, resulting in the deaths of 301 people and marking it as the deadliest coal mine disaster of the 21st century. [10].

The involvement of O_2 is one of the elements of SCC. When adequate oxygen interacts with coal and heat dissipation through conduction and convection is limited, the accumulated heat can elevate the coal's temperature to its ignition point [29]. The presence of significant coal residue and oxygen-rich air leakage in the goaf presents a potential risk of SCC [43]. The release of pressure and the expansion of pores and fissures in the fractured coal and rock mass within the goaf lead to the

* Corresponding author.
E-mail address: jhkang@cumt.edu.cn (J. Kang).

https://doi.org/10.1016/j.fuel.2025.134341
Received 16 November 2024; Received in revised form 23 December 2024; Accepted 5 January 2025
Available online 8 January 2025

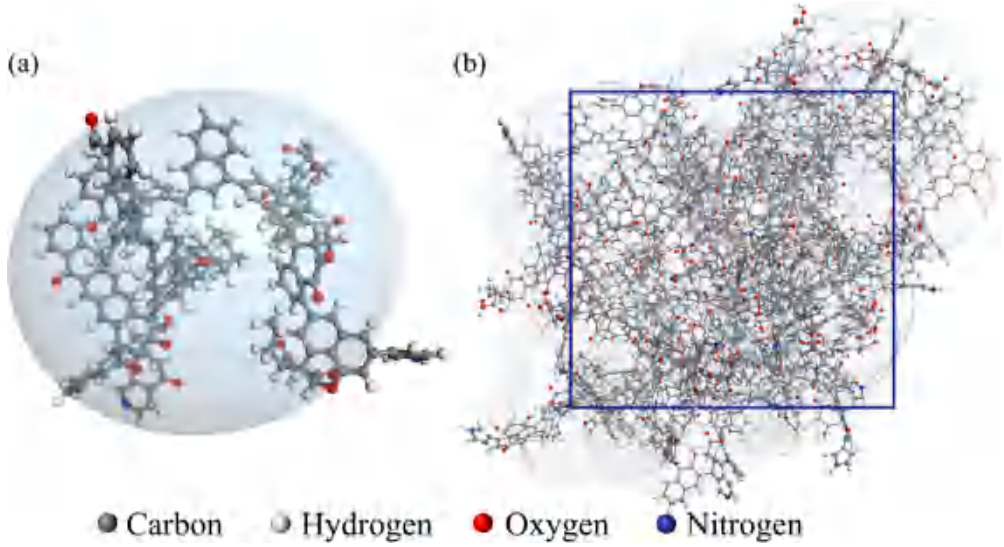

Fig. 1. Construction of anthracite molecular substrates. (a) Coal molecules constructed by Meng et al. [27]; (b) Macro molecular model of anthracite. Note: Grey – Carbon Atom; Blue – Nitrogen Atom; Red – Oxygen Atom; White – Hydrogen Atom; Yellow – Sulfur Atom.

gradual emission of gas from the coal body. This gas moves with the leakage flow field, resulting in fluctuations in CH_4 and O_2 concentrations in the environment [30]. The increase in coal temperature and variations in the proportion and partial pressure of gas components influence gas adsorption on the coal surface. When the residual methane content in the goaf coal is high, the effect of CH_4 on the coal-oxygen complex reaction cannot be ignored. In the slow desorption process of residual CH_4 in the goaf, the O_2 in the leakage flow field will invade the coal matrix under the action of concentration gradient and occupy the exposed adsorption vacancies. During this phase, the competitive adsorption of CH_4 and O_2 significantly influences the process, advancing the coal-oxygen composite reaction into a favorable development stage [31,35].

Numerous scholars have applied molecular simulation methods to examine the thermodynamics of competitive gas adsorption on coal. Dang et al. [6] utilized quantum chemical density functional theory to create a molecular model of lignite, determining that the adsorption heat ranges from 14.65 – 28.35 J/mmol for CO_2 and from 5.48 – 13.21 J/mmol for CH_4. Hao [13] investigated how combustible gases (CO, H_2, C_2H_4, and C_2H_6) in goaf affect CH_4 adsorption on coal, finding that these gases partially inhibit CH_4 adsorption. Xiang et al. [37] used GCMC and MD simulations to study the effects of adsorption configurations and oxygen-containing functional groups in coal on the adsorption of CO_2, CH_4, and H_2O. They concluded that the interaction between coal and CH_4 is primarily physical. Long et al. [23] used computational chemistry to gain insight into the microscopic adsorption mechanisms of CH_4, CO_2, and N_2 on anthracite molecules, analyzing the potential energy distribution of these gases within the adsorption system. Yu et al. [39] developed a molecular model of bituminous vitrinite. Using quantum chemistry and Monte Carlo methods, they investigated the effects of various oxygen-containing functional groups (carbonyl, ether bond, hydroxyl, and carboxyl) and electrostatic interactions on the competitive adsorption of CO_2, CH_4, and N_2. The results indicate that the hydroxyl functional group exerts the most substantial effect on adsorption capacity, whereas carboxyl has the strongest influence on adsorption selectivity. Electrostatic interactions were beneficial to the adsorption of CO_2 and N_2, but not to the adsorption of CH_4. Kim et al. [15] analyzed the adsorption characteristics of CO_2 and CH_4, and found that the adsorption potential of CO_2 was greater than that of CH_4.

In summary, while multi-component gas adsorption in coal has been extensively studied, research focusing on continuous CH_4/O_2 competitive adsorption during SCC in goaf regions is still limited. This study aims to clarify the scientific issue, by developing a molecular model of coal – CH_4/O_2 using molecular simulations like GCMC, MD, and DFT. The competitive adsorption behavior of CH_4/O_2 at different temperatures, adsorption equilibrium pressures and different component ratios is explored in detail. The adsorption amount, adsorption heat, initial adsorption potential and adsorption selectivity of CH_4/O_2 are analyzed. The radial distribution function curve (RDF) of the adsorbed gas phase relative to coal surface atoms, along with the binding energy-adsorption distance curve at functional groups, is analyzed to determine the distribution characteristics of CH_4/O_2 competitive adsorption sites. This study aims to reveal the microscopic characteristics of CH_4/O_2 competitive adsorption and the associated exothermic mechanisms in coal.

Table 1
Molecular modeling parameters and settings.

Task	Parameter	Specific value
Energy minimization	Force field	CompassIII
	Charges	Forcefield assigned
	Max.iterations	50,000
Anneal	Initial&Mid-cycle temperature	293 K ~ 593 K
	Cutoff distance	18.5 Å
	Total number of steps	50,000
AC construction	Density	1.31 g/cm^3
	Shape	Side Length = 38.8818
		Angle = 90°

2. Methodology

2.1. Molecular model

Coal molecules comprise intricate –C- skeletons, varied side chains, and irregular pore structures, forming a group of 'similar compounds' predominantly made up of organic matter. We utilize the molecular model developed by Meng et al. [27] as the base molecule, and loads 16 base molecules to form the periodic macromolecule of coal, as shown in Fig. 1(a). The molecular formula is $C_{183}H_{130}O_{20}N_2$, and the relative molecular mass is 2959.17.

Fig. 1(b) illustrates the optimized macromolecular model. The optimized molecular model shows a strong sense of spatial stereo, and the torsion amplitude at the bridge bond is close to 90°. Each branch chain shows parallel stratification, the aromatic core plane and the aliphatic

Table 2
Simulation program and groups.

Simulation Group	CH_4: O_2	Temperature/K	Pressure/MPa	Simulation Group	CH_4: O_2	Temperature/K	Pressure/MPa
#1	5: 5	273	0.02 ~ 2.0	#9	1: 9	293	0.02 ~ 2.0
#2		293		#10	2: 8		
#3		313		#11	3: 7		
#4		333		#12	4: 6		
#5		353		#13	6: 4		
#6		373		#14	7: 3		
#7		393		#15	8: 2		
#8		413		#16	9: 1		

Table 3
Physical parameters of oxygen and methane molecules.

Gas adsorbent	Critical temperature	Critical pressure	Polarizability	Ionization potential	Kinetic diameter
CH_4	190.51 K	4.6 MPa	6.541	13.79 eV	0.38 nm
O_2	154.58 K	5.04 MPa	3.211	10.6 eV	0.346 nm

group are obviously twisted, and π-π stacking appears locally [5,8,12]. Refer to Table 1 for the parameter settings.

2.2. Simulation details

The molecular simulations were conducted using MS 2023 (https://accelrys.com). A binary mixture of CH_4 and O_2 in equal proportions was used as the adsorbate to study the competitive adsorption isotherms and adsorption heat on coal molecules. Simulations were performed at pressures ranging from 0.02 MPa to 2.0 MPa and temperatures from 273 K to 413 K, covering the typical pressure and temperature conditions encountered in underground coal mines[38,42]. These include near-atmospheric pressures in depleted zones to elevated pressures in areas with residual gas or sealed conditions, as well as thermal environments relevant to the self-heating and initial stages of spontaneous combustion in coal. The temperature range was selected to simulate realistic mining conditions while avoiding significant coal oxidation, ensuring the focus remained on physical adsorption phenomena.

Besides, taking the binary mixed gas with CH_4 and O_2 ratio of 1:9, 2:8, 3:7, 4:6, 6:4, 7:3, 8:2, 9:1 as adsorbent, the competitive adsorption isotherms and adsorption heat of the two gases at 293 K on coal

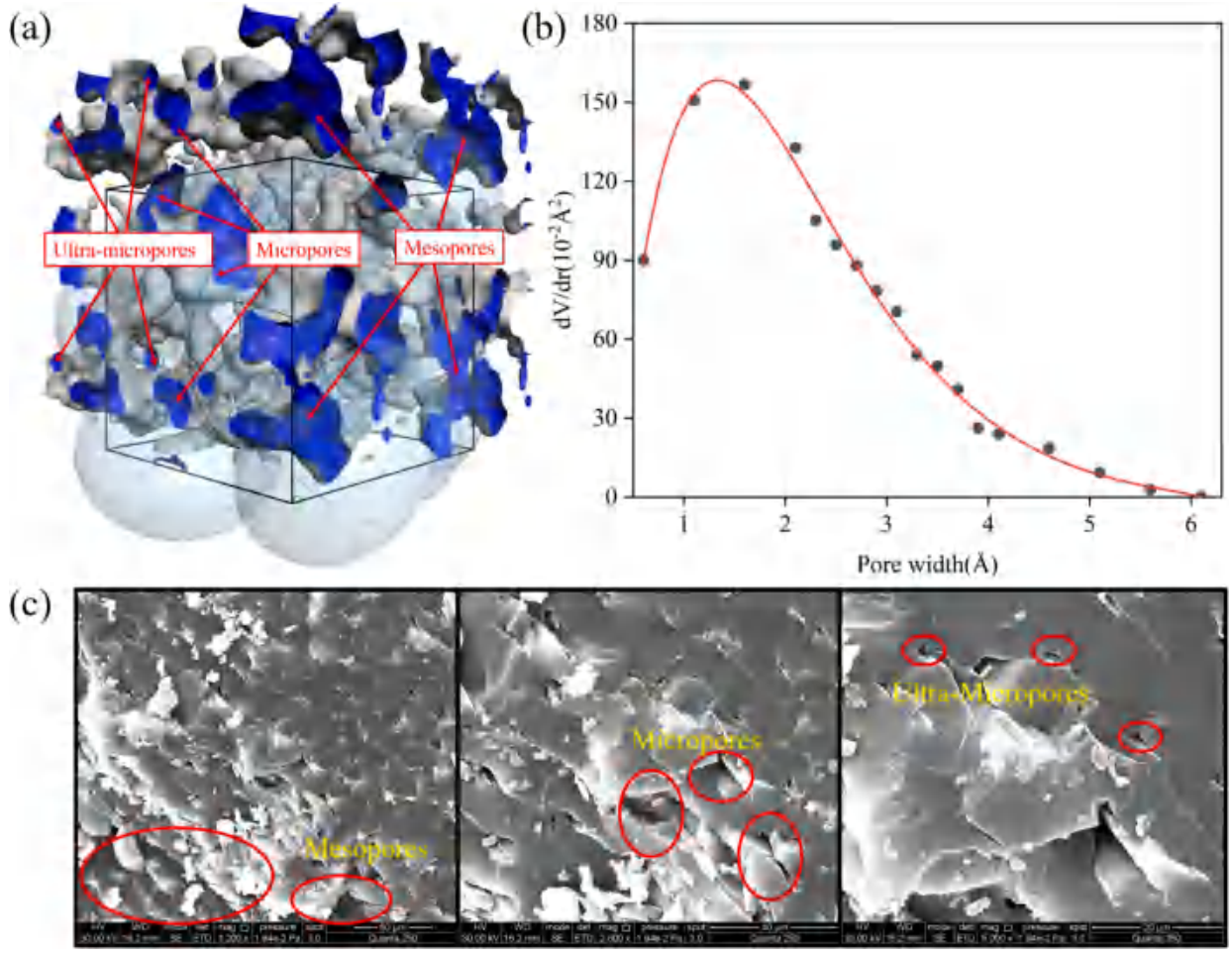

Fig. 2. Pore structure of the coal surface. (a) Connery surface of the unit cell model; (b) Pore size distribution curve; (c) Scanning electron microscope images of coal surface pores at magnifications of *1200, *2500, and *5000 in sequence [14].

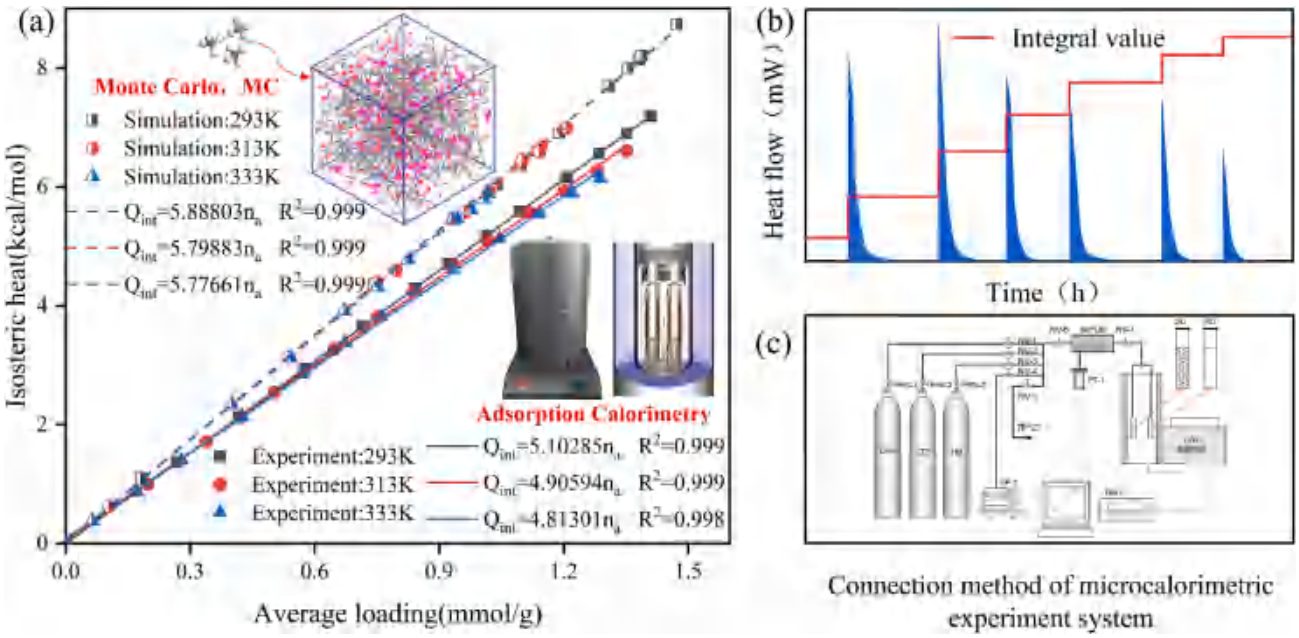

Fig. 3. Comparison of adsorption calorimetry and GCMC on isosteric heat results. (a) Comparison of different isosteric heat; (b) Experimental results of heat flow integration; (c) Microcalorimetric experiment system.

molecules under the pressure as above were studied (Table 2). This gas ratio configuration replicates the CH_4/O_2 dynamics following oxygen infiltration into the goaf. Table 3 shows some physical property parameters of CH_4 and O_2.

2.3. Adsorption models

The adsorption amount is the most important physical quantity in gas–solid adsorption research. The Langmuir model postulates a homogeneous solid surface and assumes that adsorbed molecules do not interact with each other [18]. It is the most widely used adsorption model which has the following form

$$q = \frac{abp}{1 + bp} \tag{1}$$

where q is the absolute adsorption amount at equilibrium pressure and temperature, mL/g; a is the monolayer limit adsorption amount, mL/g; b is the Langmuir constant, MPa^{-1}; p is the equilibrium pressure, MPa.

In engineering applications, the Freundlich model (Eq. (2)) is used as an empirical formula to describe heterogeneous adsorption. [11]

$$q = kp^{1/n} \tag{2}$$

where k denotes the Freundlich constant and n represents the heterogeneity factor representing the heterogeneity of the adsorbent surface.

Researchers often combine the two models to fit the adsorption on heterogeneous surfaces. The Langmuir-Freundlich (L-F) model [1,16] equation is described as follows

$$q = \frac{abp^{1/n}}{1 + bp^{1/n}} \tag{3}$$

In addition, the Toth model [33] as an empirical adaptation of the Langmuir model, effectively characterizes various adsorbent-adsorbate systems, such as hydrocarbons, carbon oxides, hydrogen sulfide, and alcohols, along with adsorbents like activated carbon and zeolites. The adsorption capacity is determined using the specified Eq. (4).

$$q = \frac{abp}{[1 + (bp)^n]^{1/n}} \tag{4}$$

3. Results

3.1. Model validation

3.1.1. Microporous morphology

Pore size distribution and specific surface area are important surface characteristics of coal and important factors affecting gas adsorption. Using nitrogen molecules with the diameter of 0.364 nm as rigid probes, the pore structure and distribution of the model surface were measured as shown in Fig. 2(a). The gray part in the figure is the Connolly surface, and the blue part is the surface pores. The surface structure parameters are obtained as: molecular volume is 35.49219 nm^3, pore volume is 2.99592 nm^3, surface area is 79.3689 nm^2, and initial porosity is 8.44 %. The model features a high specific surface area, with pore sizes predominantly ranging from 0.025 to 0.25 nm, as shown in Fig. 2(b). The results indicate that the model's surface pores consist primarily of micropores and ultra-micropores, with a small proportion of mesopores. The pore structure is densely packed and uniformly distributed [20]. It is consistent with the characteristics of the actual coal surface pores as shown in Fig. 2(c), which verifies the rationality of the surface structure of the model.

3.1.2. Adsorption calorimetry and GCMC

To validate the accuracy of the coal molecular model's physical and chemical properties, preliminary thermodynamic experiments on CH_4 adsorption in coal were conducted using the GCMC method and adsorption microcalorimetry. These experiments were performed at ambient temperatures of 293 K, 313 K, and 333 K, under pressure gradients of 0.1–2 MPa. As depicted in Fig. 3(c), the adsorption microcalorimetry experimental system comprises an adsorption heat measurement device, a volumetric adsorption apparatus, a data acquisition unit, and a gas pathway system. The gas adsorption amount is measured by the volumetric method, and the adsorption heat can be obtained by baseline integration of the heat flow signal recorded during the experiment, as shown in Fig. 3(b). As the adsorption and reference cells of the adsorption calorimeter are continuously linked, the measured heat compensates for deviations due to gas expansion work, allowing the experimental calorific value to be considered as the integrated heat.

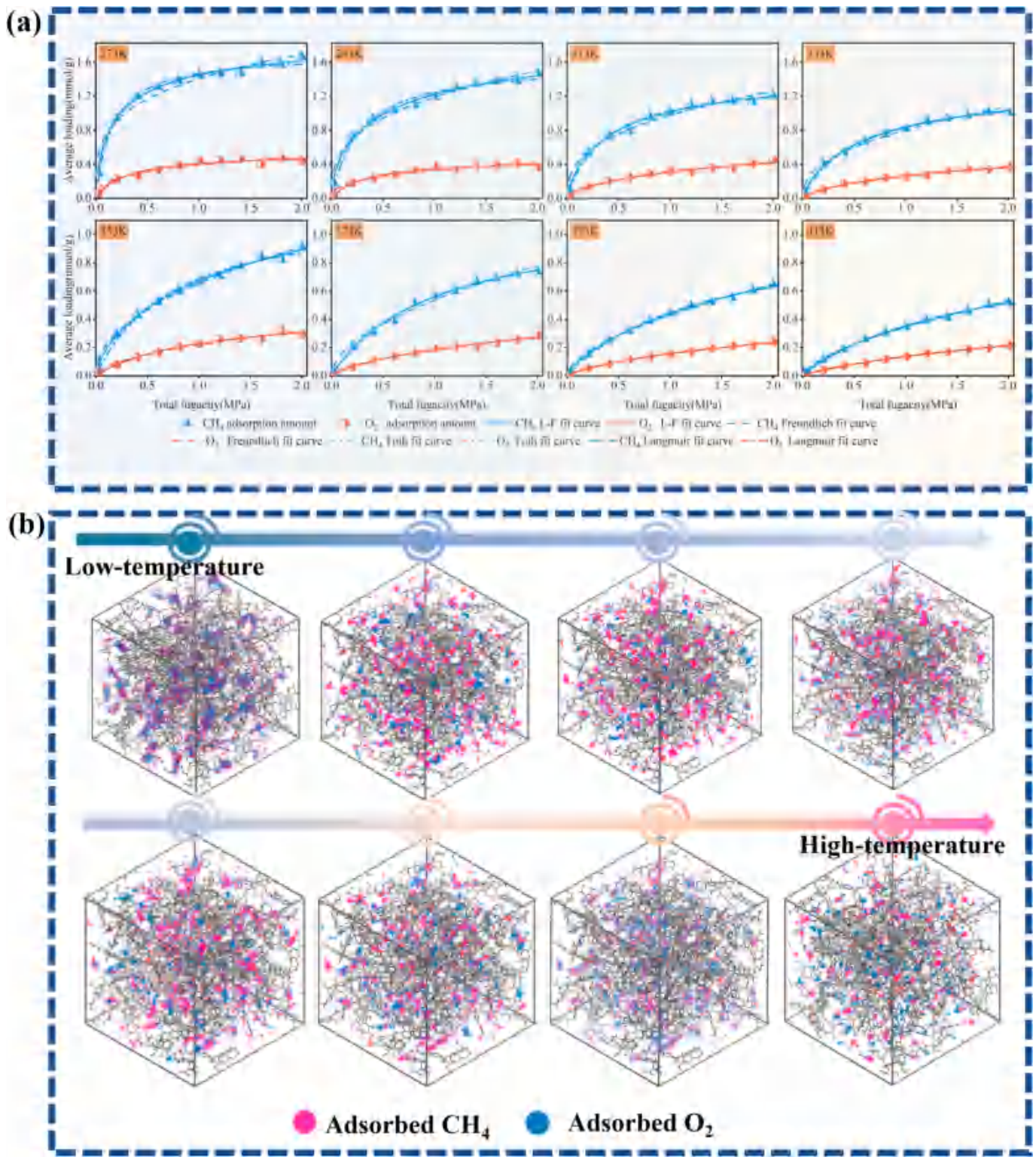

Fig. 4. Competitive adsorption behavior of CH_4 /O_2 at varying temperatures (a)Isothermal adsorption curves of CH_4 /O_2 at varying temperature fitted with four adsorption models; (b) Density distribution of adsorbate at varying temperature.

The integral heat (Q_{int}) versus adsorption amount (n_a) curve was drawn in Fig. 3(a). The slope of each curve is the isosteric adsorption heat of gas adsorbed by coal under certain temperature. The simulation curves closely align with the experimental results, both demonstrating a strong linear increase with $R^2 \geq 0.998$. The average isosteric adsorption heat obtained by molecular simulation is about 5.8212 kcal/mol, compares with 4.9406 kcal/mol obtained by adsorption microcalorimetry test, with a difference of 0.8806 kcal/mol. The deviation is almost constant at 15.127 % of the simulation value. The error may arise from the energy loss caused by heat conduction of gas flowing through the steel pipe in the microcalorimetry test, and the effects of some metal atoms and small molecular compounds doped in coal on the gas adsorption. Due to the proportional relationship between energy loss and adsorption amount, in this work the binding energy multiplied by

Table 4
Fitting parameters for various adsorption models across varying temperatures.

Components	temperature	L-F				Toth			
		a	*b*	*n*	R^2	*a*	*b*	*n*	R^2
CH_4	273 K	1.968	2.826	1.433	0.994	2.139	16.125	0.530	0.994
	293 K	2.134	1.348	1.573	0.993	2.551	9.88261	0.431	0.999
	313 K	1.585	1.794	1.239	0.993	1.736	4.065	0.638	0.993
	333 K	1.498	1.261	1.218	0.996	1.688	2.420	0.639	0.990
	353 K	1.884	0.551	1.422	0.995	3.383	1.708	0.369	0.995
	373 K	1.150	0.947	1.023	0.995	1.093	0.998	1.042	0.995
	393 K	1.720	0.343	1.286	0.998	3.803	0.469	0.396	0.998
	413 K	1.402	0.333	1.215	0.997	2.708	0.372	0.464	0.997
O_2	273 K	0.564	2.561	1.152	0.956	0.557	3.843	0.863	0.954
	293 K	0.480	2.483	1.092	0.948	0.481	3.235	0.889	0.958
	313 K	1.855	0.199	1.737	0.979	10.236	1.749	0.184	0.981
	333 K	1.017	0.350	1.448	0.990	2.725	0.903	0.303	0.990
	353 K	0.493	0.856	1.078	0.982	0.514	1.013	0.844	0.981
	373 K	1.599	0.130	1.480	0.989	13.889	0.164	0.208	0.989
	393 K	0.804	0.241	1.287	0.996	2.668	0.235	0.342	0.996
	413 K	0.657	0.263	1.140	0.999	1.199	0.227	0.539	0.998

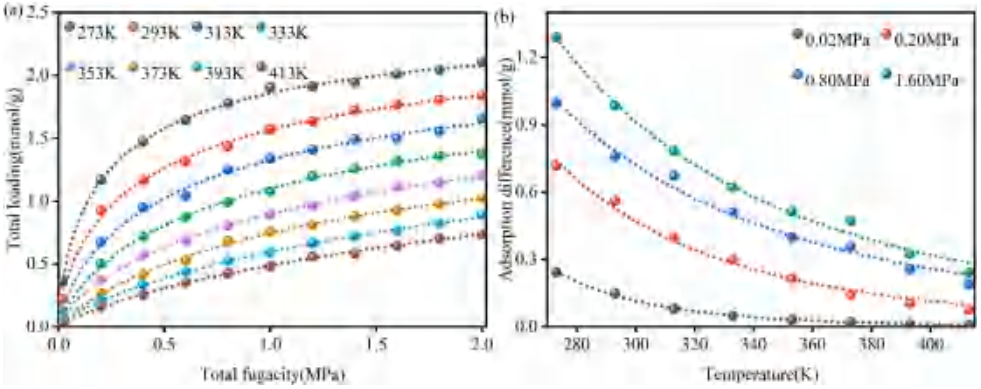

Fig. 5. Total adsorption amount and adsorption difference in adsorption amount of multi-component gas with equal proportion at different temperature. (a) Curve of total adsorption capacity changing with pressure; (b) Curve of adsorption difference changing with temperature.

84.873 % will be used as the adsorption heat value for data correction.

3.2. Analysis of multi-component gas adsorption across varying temperatures

Fig. 4 illustrates the isothermal adsorption curves for CH_4/O_2 mixtures on coal molecules across varying temperatures. Each adsorption isotherm for CH_4 and O_2 corresponds to a Type I isotherm. With rising temperatures, the adsorption amount gradually decreases, necessitating higher equilibrium pressure for the gas to achieve saturated adsorption. Additionally, the adsorption capacity of CH_4 in the mixture significantly exceeds that of O_2. At 273 K and 2 MPa, the saturated adsorption capacity of CH_4 is 3.82 times that of O_2, decreasing to 2.22 times as the temperature rises to 413 K. Furthermore, the fitting results for the four adsorption models indicate that both the Langmuir and Freundlich models achieve R^2 values greater than 0.93; the L-F model and Toth models achieve R^2 values greater than 0.95 (Table 4). The fitting accuracy ranks as L- F model > Toth model > Langmuir model > Freundlich model.

Fig. 4.b describes the adsorption phase density distribution of CH_4/O_2 on the coal surface at varying temperatures. The distribution reveals a non-uniform adsorption pattern of CH_4 and O_2, which can be attributed to the heterogeneous pore structure and the presence of diverse functional groups on the coal surface. At lower temperatures, gas molecules preferentially accumulate at adsorption sites, resulting in a higher density. Additionally, a greater overlap of adsorption sites between the two gases is observed. As the temperature increases, the adsorbed gas molecules become more thermally active and energetic, leading to partial desorption as some molecules overcome the adsorption energy barrier. Consequently, the adsorption phase density decreases with increasing temperature.

To facilitate a clearer comparison of the adsorption capacities of the two gases on the coal surface, the adsorption differential between them under identical conditions was calculated (*adsorption difference* = q_{CH4}-q_{O2}). Fig. 5 shows the total isothermal adsorption curve of multi-component gas with equal proportion and the adsorption difference of the two components. The isothermal adsorption curve of mixed gas also shows the type I of adsorption isotherm. The total adsorption amount decreases with the increasing temperature. At 2 MPa, the total adsorption decreases from 2.015 mmol/g at 273 K to 0.734 mmol/g at 413 K. The downward trend gradually slows down and the equilibrium pressure shifts backward, indicating that a higher pressure is required to achieve saturated adsorption in a high temperature environment. The adsorption difference increases with rising temperature or decreasing pressure, highlighting that methane adsorption is more sensitive to these changes, with notable variations observed between 273 K and 333 K.

3.3. Analysis of multi-component gas adsorption across varying ratios

Fig. 6 illustrates the competitive adsorption of each component by calculating the adsorption capacities of the CH_4/O_2 gas mixture on coal molecules at varying ratios ($\varphi_0 = CH_4{:}O_2$). The adsorption amount of O_2 is negatively correlated with φ_0, while the opposite result holds for CH_4. Variations in φ_0 significantly impact CH_4 levels. In other words, a high proportion of CH_4 will interfere with the adsorption of O_2. At φ_0 = 2:8, the adsorption isotherms for CH_4 and O_2 nearly coincide, suggesting

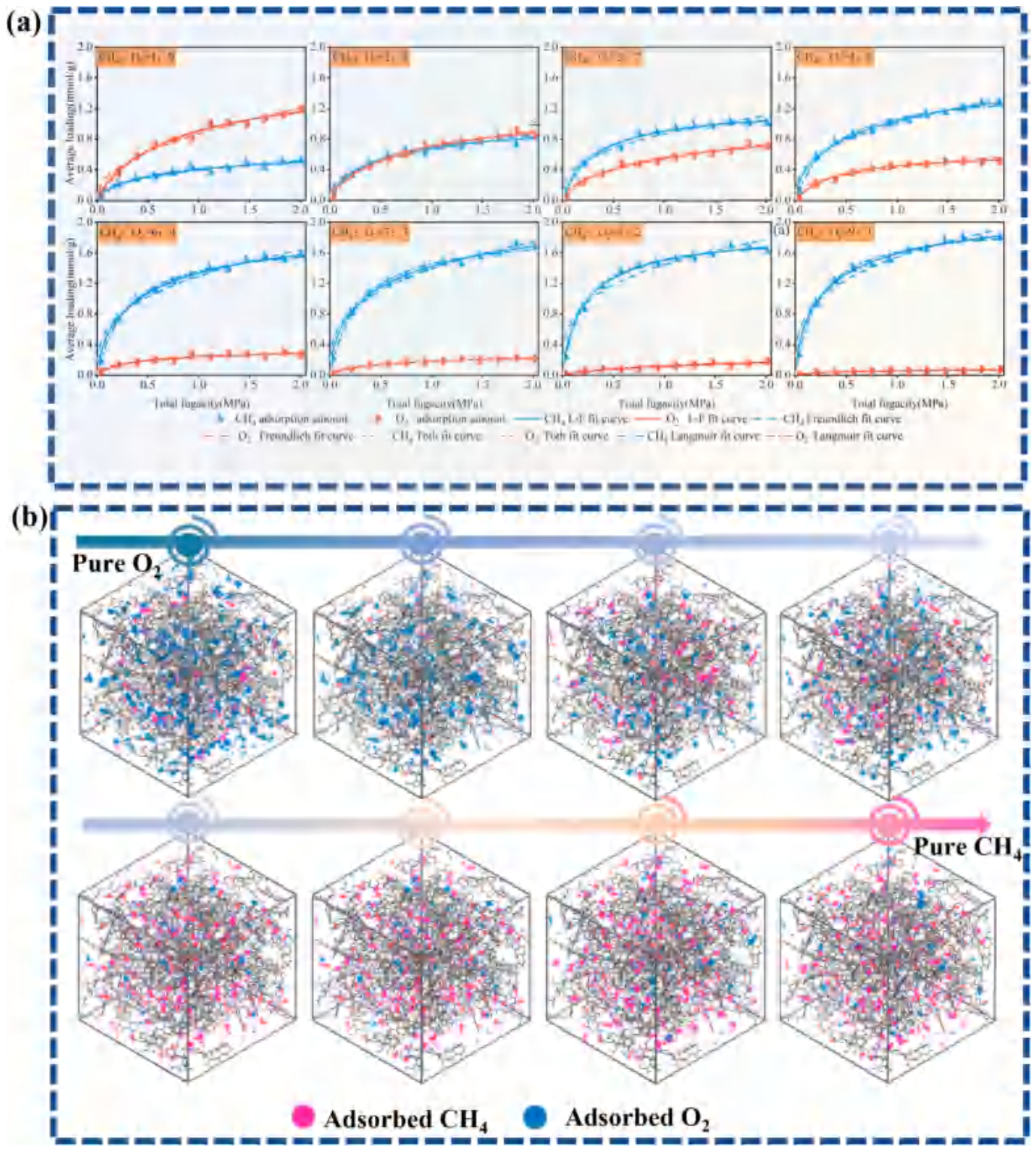

Fig. 6. Competitive adsorption behavior of CH_4 /O_2 with varying ratio under pressure gradient. (a) Isothermal adsorption curves of CH_4 /O_2 with varying ratio under pressure gradient and four adsorption model fitting curves; (b) Density distribution of adsorbate with varying ratio at 2.0 MPa.

equal competition between the two gases for adsorption sites on the coal surface. After $\varphi_0 > 8{:}2$, the adsorption isotherm of O_2 changes linearly in the range of 0.02 MPa ~ 2 MPa, and the adsorption amount changes very slowly with pressure. In addition, it can be seen from Table 5 that when $\varphi_0 > 8{:}2$, the fitting results for O_2 are suboptimal, with the L-F and Toth models showing R^2 values greater than 0.841. In most instances, the two models, with R^2 values exceeding 0.95, effectively fit the adsorption quantities of each component in competitive adsorption scenarios.

Fig. 6.b describes the adsorption phase density distribution of ch4/o2 on the coal surface with varying ratio at 2.0 MPa. As the proportion of CH_4 increases, the adsorption sites for O_2 are rapidly displaced by CH_4. Notably, at a CH_4/O_2 molar ratio of 7:3 to 8:2, the overlap of adsorption sites between CH_4 and O_2 reaches its maximum. This phenomenon arises

Table 5
Fitting parameters of different adsorption models with different ratio.

Components	temperature	L-F				Toth			
		a	b	n	R^2	a	b	n	R^2
CH_4	1:9	0.867	0.867	1.524	0.964	1.265	5.092	0.377	0.966
	2:8	1.105	1.618	1.263	0.969	1.217	3.820	0.622	0.974
	3:7	1.287	2.326	1.161	0.988	1.316	3.874	0.782	0.988
	4:6	2.198	0.895	1.621	0.995	3.277	8.401	0.341	0.996
	6:4	2.168	1.604	1.411	0.996	2.547	7.154	0.494	0.996
	7:3	2.480	1.351	1.562	0.995	3.151	11.186	0.402	0.995
	8:2	1.959	3.267	1.021	0.992	2.026	7.094	0.721	0.992
	9:1	2.350	2.087	1.415	0.996	2.644	10.195	0.515	0.997
O_2	1:9	1.820	0.982	1.209	0.989	2.141	1.722	0.621	0.988
	2:8	1.407	0.990	1.322	0.990	1.785	2.634	0.508	0.990
	3:7	1.472	0.596	1.515	0.981	2.623	2.848	0.339	0.981
	4:6	0.626	2.563	0.977	0.991	0.591	2.185	1.22	0.992
	6:4	0.354	2.139	1.197	0.958	0.372	4.154	0.712	0.951
	7:3	0.309	1.422	1.254	0.976	0.346	3.176	0.615	0.976
	8:2	2.458	2.713	1.28	0.956	0.259	4.733	0.651	0.915
	9:1	0.111	1.038	1.45	0.841	0.153	4.860	0.416	0.841

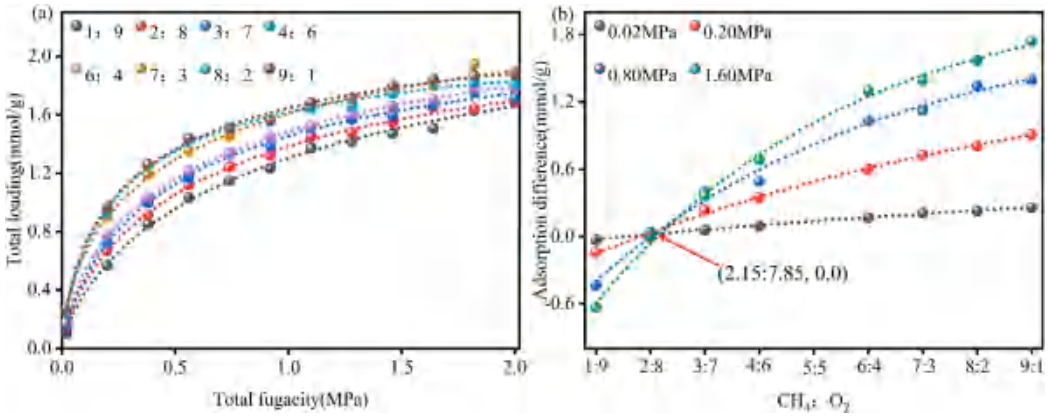

Fig. 7. Total adsorption amount and difference in adsorption amount of multi-component gas with different ratios. (a) Curve of total adsorption capacity changing with pressure; (b) Curve of adsorption difference changing with component ratio.

from the comparable adsorption capacities of CH_4 and O_2 within this specific ratio range. When one gas becomes dominant in proportion, it further monopolizes the shared adsorption sites. In contrast, the characteristic adsorption sites, due to their specificity, are less affected by changes in gas composition.

Fig. 7 shows the isothermal adsorption curve of the gas mixture on coal molecules at different ratios and the difference curve of the adsorption of the two components. The total adsorption amount decreases with the increasing temperature, but the change is smaller than that of the temperature. At the pressure of 2 MPa, the total adsorption amount decreases from 1.877 mmol/g with φ_0 = 1:9 to 1.706 mmol/g with φ_0 = 9:1. This suggests that CH_4 and O_2 primarily share adsorption sites on coal molecules. If only the φ_0 changes, the displacement adsorption occurs at the shared adsorption sites, the dominant adsorbed molecules will further occupy the adsorption sites, and other adsorbate molecules will be replaced into the environment. In addition, as pressure increases, the adsorption capacity of CH_4 rises substantially more than that of O_2. For the pressure of 0.02 MPa to 2 MPa, the difference in adsorption amount between φ_0 = 1:9 and φ_0 = 9:1 change from 0.27 mmol/g to 2.37 mmol/g. The adsorption of CH_4 is more sensitive to variations in temperature and pressure, aligning with findings from competitive adsorption studies at varying temperatures. We observed that under varying pressures, the curves of adsorption difference exhibit a focal point at the coordinate (2.15: 7.85, 0.0). This indicates that the adsorption capacities of CH_4 and O_2 are equivalent at this specific ratio, and this phenomenon remains consistent regardless of pressure changes. It suggests that, although CH_4 generally exhibits a significantly higher adsorption capacity compared to O_2, enhancing its adsorption advantage requires an increase in its molar proportion rather than an increase in absolute partial pressure.

4. Discussion

4.1. Competitive adsorption selectivity

Adsorption selectivity is usually used to characterize the competitive adsorption relationship of porous media to different adsorbates. The adsorption selectivity factor of component A to component B in a multi-component gas mixture is expressed as

$$S_{A/B} = \frac{x_A/x_B}{y_A/y_B} \tag{5}$$

In the adsorbed phase, x_A / x_B represent the mole fractions of components A/B, respectively, while y_A / y_B denote the mole fractions of components A / B in the free phase. If $S_{A/B}$ less than 1, it means that B has a higher adsorption priority and B is more likely to occupy the adsorption sites of the pores on the adsorbent surface.

Fig. 8 gives the binary adsorption selectivity of CH_4/O_2 ($S_{CH4/O2}$). As shown in Fig. 8(a), the value of $S_{CH4/O2}$ is smaller for the low pressure, indicating that the adsorption competitiveness of O_2 is relatively smaller than that for the high pressure. $S_{CH4/O2}$ ncreases with pressure, as at high pressures, the adsorption capacity of coal pores for CH_4 molecules approaches its saturation limit, while O_2 remains in an unsaturated state. At this stage, the adsorption competitiveness of O_2 becomes greater than

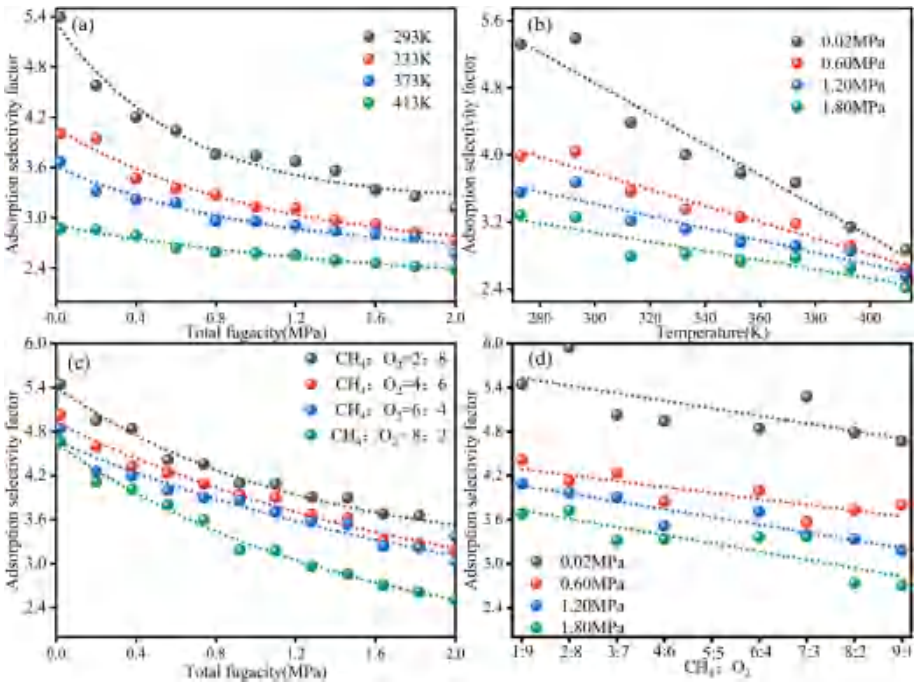

Fig. 8. Selectivity of binary adsorption of CH_4 / O_2 . (a) Pressure-dependent variation of the adsorption selectivity factor at varying temperatures; (b) Temperature-dependent variation of the adsorption selectivity factor at varying pressures; (c) Pressure-dependent variation of the adsorption selectivity factor at varying component ratios; (d) Component ratio-dependent variation of the adsorption selectivity factor at varying pressures.

at lower pressures, yet the value of $S_{CH4/O2}$ remains below 1, signifying that coal's adsorption selectivity for O_2 is still less than that for CH_4, even under these conditions.

Fig. 8(b) and (d) describe the adsorption selectivity of CH_4 to O_2 when $\varphi_0 = 1$ and when φ_0 increases from 1/9 to 9/1 at a temperature of 293 K, respectively. The S_{CH_4/O_2} shows a decreasing trend as the ratio increases. Elevated CH_4 levels enhance the preferential adsorption of O_2 on coal surfaces. Due to the significantly higher adsorption of CH_4 compared to O_2, the selectivity for O_2 adsorption over CH_4 is enhanced, facilitating O_2 adsorption. Oxidation of the coal sample increases the proportion of large pores, enhancing the interaction between CH_4, O_2, and coal surface functional groups. This leads to an increase in adsorption sites due to stronger interactions between gas molecules and the coal surface. As the saturated adsorption of O_2 increases, both the temperature and the oxidation level of coal rise.

4.2. Initial adsorption potential energy

The affinity distribution function (ADFs) describes the energy spectrum of adsorption sites by linking adsorption isotherm parameters with energetic characteristics [3]. ADFs allow for comparison of binding site distributions with varying adsorption potentials between coal surfaces and gas molecules, providing a measure of surface heterogeneity. [4]:

$$P(E) = \frac{a(bp)^{\frac{1}{n}}}{nRT}\exp\left(\frac{-E}{nRT}\right)\left[1 + (bp)^{\frac{1}{n}}\exp\left(\frac{-E}{nRT}\right)\right]^{-2} \quad (6)$$

where p is the equilibrium pressure, MPa; a is the monolayer limit adsorption amount, L/Kg; b is the adsorption constant, MPa^{-1}; n is the heterogeneity factor; T is temperature, K; R is Avogadro constant and E^* is net energy.

Fig. 9 shows the ADFs of CH_4 and O_2 on the coal surface. Both curves exhibit a "double-peak" skewed distribution, as explained by the micropore filling theory [45]. The coal molecular model exhibits significant physical heterogeneity, characterized by surfaces formed by the inner and outer layers of ultra-micropores and micropores. There are strong adsorption areas and weak adsorption areas on the coal surface. The low peak position is the strong adsorption area where the gas molecules are in the most stable adsorption configuration. The high peak position is the weak adsorption area where the adsorption energy is relatively low, and there are more adsorbed phase molecules. During single-component adsorption, the gas molecules are filled from the strong adsorption area to the weak adsorption area in sequence. The dynamic radius and polarity of gas molecules are the primary factors influencing adsorption. Under identical conditions, the adsorption capacities of pure CH_4 and O_2 are comparable. During competitive adsorption, the heterogeneous characteristics of coal surface determine the priority of adsorption of gas components. Methane is in an advantageous position in the competition with oxygen in the micropore strong adsorption area, occupying most of the strong adsorption area sites. The heterogeneous structure of the coal surface minimally influences gas molecule adsorption in weak adsorption areas, resulting in limited competitive adsorption behavior.

Table 6 shows the initial adsorption potential (IAP) values of CH_4 and O_2. It can be seen that the stability of CH_4 in coal is higher than that of O_2. The IAP of the CH_4 and O_2 system initially rises and then falls as the temperature increases from 273 K to 393 K. In a multi-component adsorption system, the adsorption potential is also influenced by the gas molar fraction. With the proportion of CH_4 increases from 0.2 to 0.8, the IAP of CH_4 increases from −5.65 kcal/mol to −5.15 kcal/mol (the initial adsorption potential of CH_4 improves by 8.8 %), and the IAP of O_2 decreases from −4.15 kcal/mol to −4.75 kcal/mol (the initial adsorption potential of O_2 decreases by 14.5 %). This suggests that a higher CH_4 concentration promotes O_2 adsorption on coal, consistent with the adsorption selectivity analysis results.

4.3. Thermodynamic characterization of competitive adsorption

Physical adsorption is an exothermic process characterized by the release of heat, known as adsorption heat (AH). In GCMC, fluctuation theory in MD at a constant temperature allows for the calculation of the isosteric heat of adsorption (IAH). [9]. Fig. 10 shows the variation trend

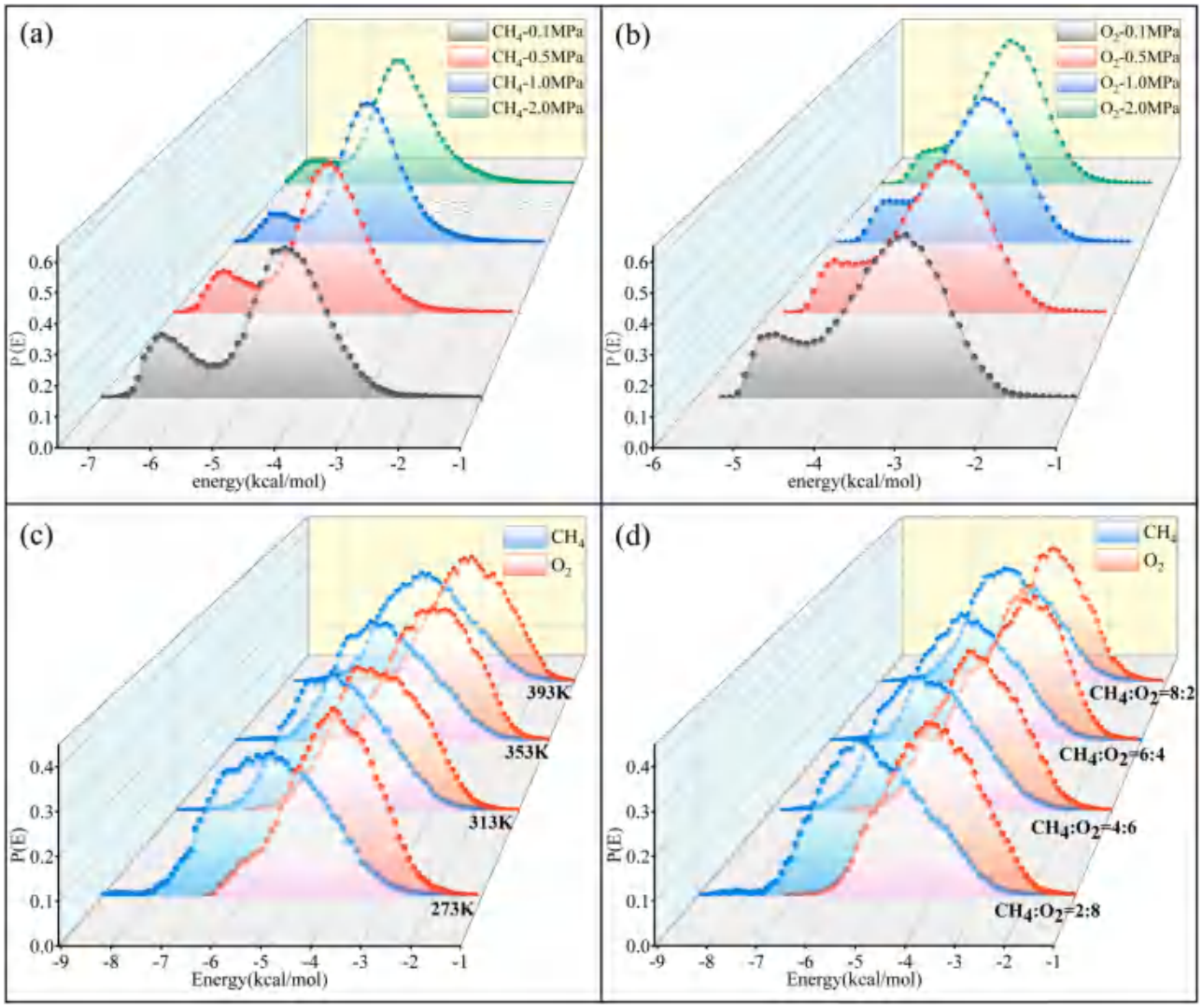

Fig. 9. *P(E)* of the L–F model for different values of the constants a/b/n (a) ADF curve for CH_4 adsorption; (b) ADF curve for O_2 adsorption; (c) ADF curves of CH_4 /O_2 competitive adsorption at different temperatures; (d) ADF curves of CH_4 /O_2 competitive adsorption at different component ratios.

Table 6
The IAP values of CH_4 and O_2 .

Adsorption conditions	IAP values/ (kcal/mol)		Adsorption conditions	IAP values/ (kcal/mol)	
$\varphi_0 = 1$	CH_4	O_2	293 K	CH_4	O_2
273 K	−5.55	−4.15	2:8	−5.65	−4.15
313 K	−5.85	−4.45	4:6	−5.45	−4.35
353 K	−5.55	−3.95	6:4	−5.35	−4.35
393 K	−5.25	−3.85	8:2	−5.15	−4.75

of IAH with temperature, pressure, and component ratio. There is a slight fluctuation in the isosteric adsorption heat of the two gases exhibits minor fluctuations due to the heterogeneous nature of the coal surface [17]. CH_4 has a larger adsorption heat, which is related to the larger polarizability and ionization potential of CH_4 molecules [46]. Greater molecular polarizability and ionization potential lead to stronger dispersion and induction forces, which in turn increase the AH.

Fig. 10(a) illustrates the competitive adsorption of CH_4 and O_2 at various temperatures. The AH of both gases varies and declines as pressure and temperature rise. The adsorption heat of CH_4 decreases from 6.06 kcal/mol at 273 K and 0.02 MPa to 5.65 kcal/mol at 413 K and 2 MPa. Similarly, the AH of O_2 decreases from 4.87 kcal/mol to 4.51 kcal/mol. Fig. 10(b) illustrates the competitive adsorption of CH_4 and O_2 at varying ratios. The CH_4 AH remains relatively stable, fluctuating between 5.77 and 6.05 kcal/mol, regardless of the CH_4 proportion. In contrast, the AH of O_2 shows a significant increase when the CH_4 proportion exceeds 0.6, with most values surpassing 4.65 kcal/mol.

4.4. Characterization of adsorbate microdistribution

The radial distribution function (RDF) characterizes the microstructure of particles by comparing the local density of the system to the average volume density. The RDF reflects the aggregation characteristics of particles and describes how the heterogeneous surface of the adsorbent influences the competitive adsorption of CH_4 and O_2 in the system. [26]. The first action peak can characterize the affinity between microscopic particles. The RDF calculation method is as follows.

$$g_{a-b}(r) = \frac{dN}{4\pi\rho r^2 dr} = \frac{1}{4\pi\rho r^2 \delta_r} \frac{\sum_{t=1}^{T}\sum_{j=1}^{N} \Delta N(r \to r + \delta_r)}{Nt} \tag{7}$$

where $g_{a\text{-}b}(r)$ indicates the aggregation degree of particles; r is the center radius of the adsorbate particle a from the target atom b on the adsorbent surface, nm; N represents the number of particles; ρ is the density of a, *amount of particles/nm*^{3}; t is the step sequence; j is the particle ordinal

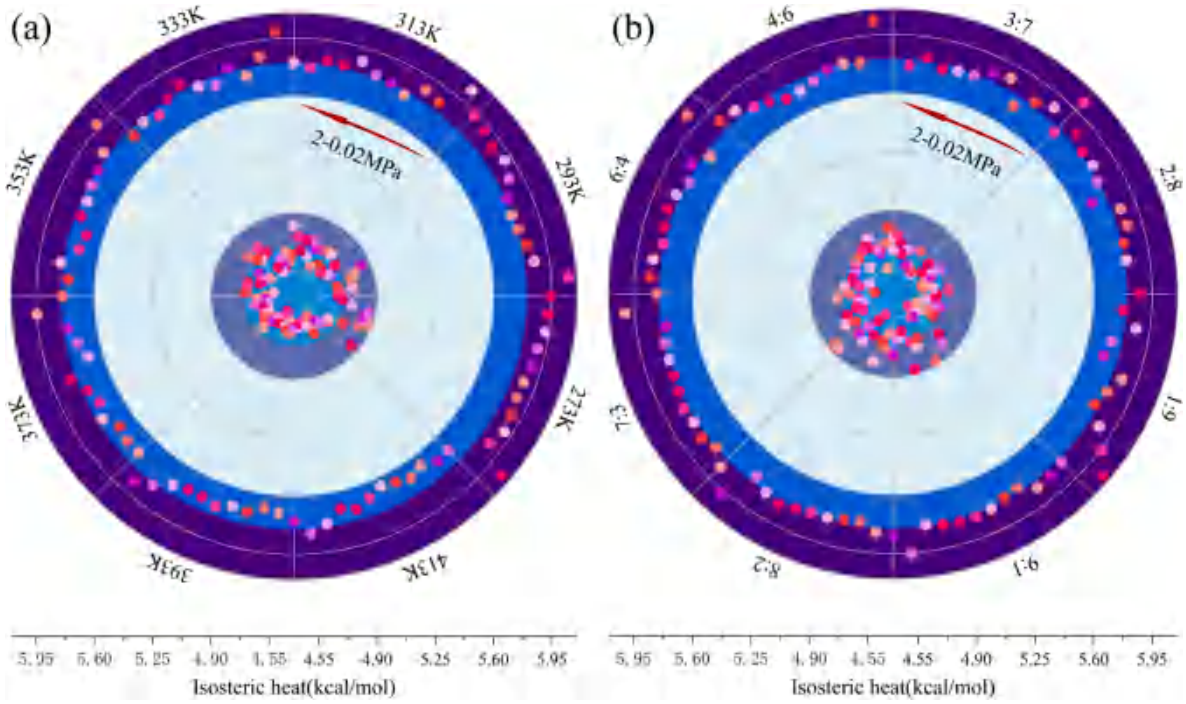

Fig. 10. Comparison of the CH_4 / O_2 IAH. (a) IAH of CH_4 /O_2 at different temperatures; (b) IAH of CH_4 /O_2 with different component ratios.

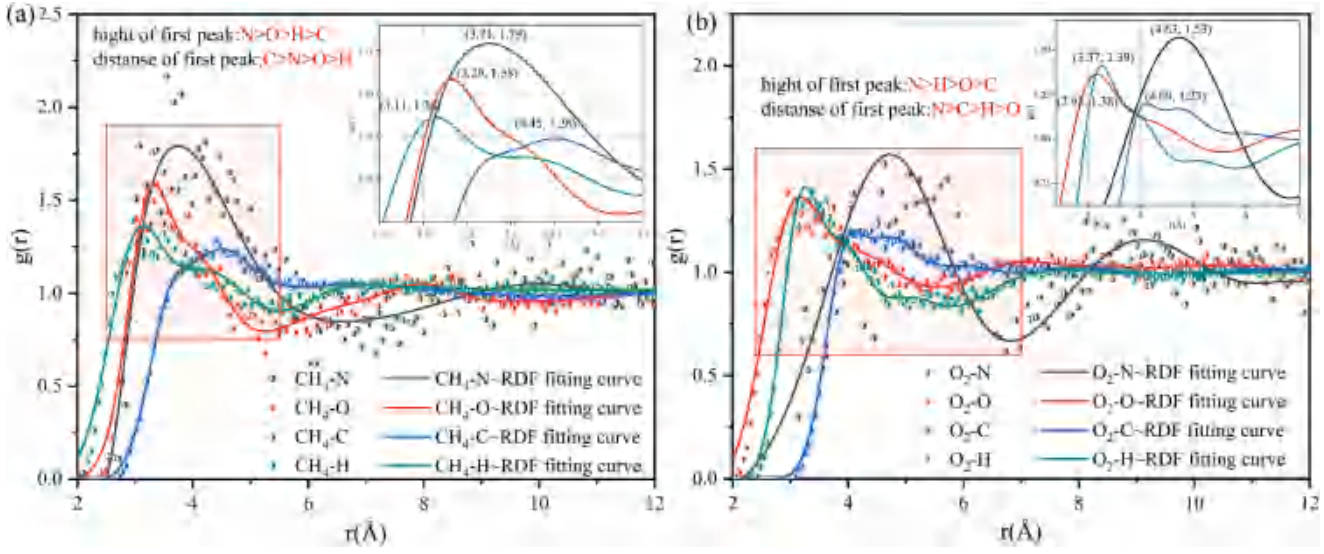

Fig. 11. RDFs between CH_4 /CO_2 and atoms in the coal models. (a) RDF curves between adsorbed CH_4 molecules and C/H/O/N atoms; (b) RDF curves between adsorbed O_2 molecules and C/H/O/N atoms.

number; $\Delta N(r \rightarrow r+\delta_r)$ is the amount of a in the range of $r \rightarrow r+\delta r$; δr is the set distance difference; and t is the total calculation time.

Fig. 11 is the RDF diagram between the CH_4 and O_2 and the atoms on the surface of coal molecules. It can be seen that CH_4 has the interaction peaks with the atom N at 3.71 Å, O at 3.29 Å, C at 4.45 Å and H at 3.11 Å, and the size of the peaks is 1.79 (N) > 1.58 (O) > 1.36 (H) > 1.26 (C). O_2 has the interaction peaks with the atom N at 4.63 Å, O at 2.95 Å, C at 4.09 Å and H at 3.37 Å, and the size of the peaks is 1.53 (N) > 1.39 (H) > 1.38 (O) > 1.24 (C). The higher the peak, the stronger the interaction between the gas molecule and the adsorption site, and the closer the connection between the atoms. The RDF curve indicates that the adsorption equilibrium distance for both gases on the coal molecule surface is 3 ~ 5 Å, with similar position and shape of action peaks for C and H atoms. This indicates that CH_4 and O_2 share the adsorption sites at C and H atoms, which is the main place for O_2 to replace CH_4. The mass of carbon and hydrogen atoms, which make up 78.61 % of coal molecules, suggests that most adsorption sites on the coal surface are available for CH_4 and O_2 competition. This explains why the total adsorption capacity of the mixed gas shows little variation with different component ratios. In addition, the action peaks of CH_4 and O_2 at N and O atoms are more obvious and the differences are large, indicating that there are more specific adsorption sites at N and O atoms. The RDF peak of CH_4 at N and O atoms surpasses that of O_2, indicating that methane exhibits dominant competitive adsorption.

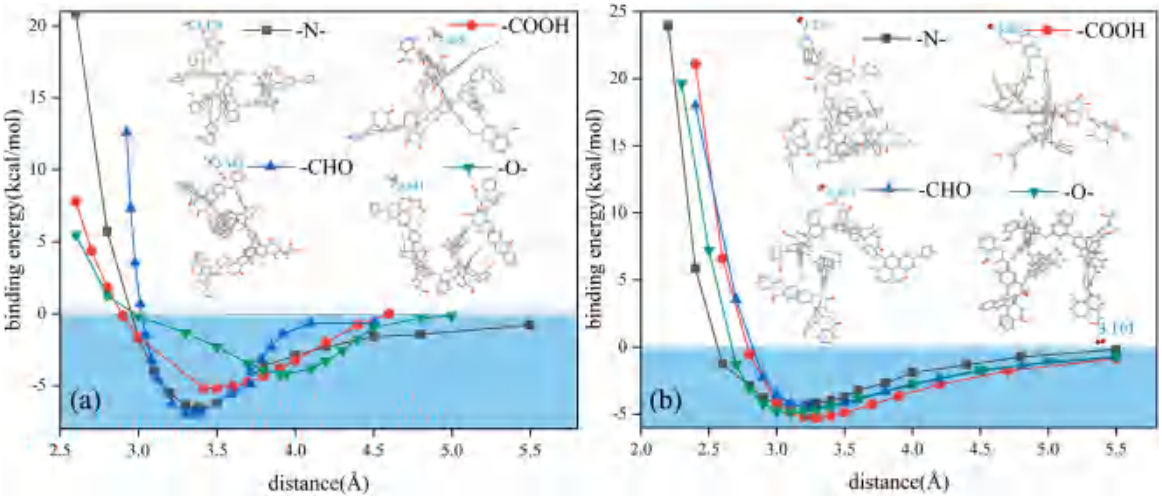

Fig. 12. Binding energy between CH_4 /CO_2 and functional group in the coal models. (a) Binding energy and adsorption configurations variation of CH_4 at functional groups; (b) Binding energy and adsorption configurations variation of O_2 at functional groups.

Table 7
Binding energy parameters for stable adsorption at different functional groups.

Functional groups	Average binding energy (kJ/mol)		Average adsorption distance (Å)	
	CH_4	O_2	CH_4	O_2
−N-	−6.580	−4.375	3.378	3.224
–COOH	−5.183	−5.251	3.418	3.283
–CH = O	−7.057	−4.611	3.343	3.263
−O-	−4.196	−4.902	3.941	3.101

4.5. Binding energy at functional groups

Density functional theory (DFT) can be used to calculate the adsorption configuration and energy at nitrogen and oxygen functional groups. Spin-unrestricted all-electron DFT calculations are performed using the Perdew-Burke-Ernzerhof (PBE) functional within the generalized gradient approximation (GGA). The OBS method in Grimme and PW91 is used for dispersion correction in DFT, and the dual numerical polarization (DNP) basis set is employed to expand the electronic wave function. The Green model (DFT-D2) is employed to accurately describe van der Waals interactions during the adsorption of mixed gases near coal molecule functional groups. The formula used to calculate the adsorption energy is:

$$E_{ads} = E_{adsorbate} + E_{surf} - E_{adsorbate+surf} \quad (8)$$

where E_{ads} is the adsorption energy, $E_{adsobate}$ is the total energy of the gas molecules, E_{surf} is the energy of the anthracite molecules, $E_{sdsorbate+surf}$ is the energy of the gas in stable the adsorption system at the functional group position.

Functional groups in coal provide sites for gas attachment and are also the “cradle” of coal-oxygen bonding reactions. Fig. 12 illustrates the binding energy curves as a function of the adsorption distance for CH_4 and O_2 at the coal surface’s functional groups, depicting their stable adsorption configurations. The curves illustrate the stable adsorption configurations of CH_4/O_2 on adsorption sites with O-containing functional groups (–COOH, –CH = O, −O-) and N-containing functional groups (−N-).Despite similar adsorption directions of CH_4 and O_2 at functional groups, their adsorption distances and energies differ significantly. [19,41].

The calculation parameters of average binding energy and average adsorption distance are shown in Table 7. The calculated distance from CH_4 to the functional group ranges from 3.343 to 3.941 Å. The distance from O_2 to the functional group ranges from 3.101 Å to 3.283 Å. Correspondingly, the binding energy between CH_4 and the functional group ranges from −4.196 kcal/mol to −7.057 kcal/mol, and the binding energy between O_2 and the functional group ranges from −4.375 kcal/mol to −5.251 kcal/mol. The greater average adsorption distance and binding energy of CH_4 compared to O_2 suggest a stronger interaction between CH_4 and the coal surface’s functional groups. For CH_4, the binding energy is (–CH = O) > (−N-) > IAH > (–COOH)>(−O-); while for O_2, the binding energy is (–COOH) > (−O-) > (–CH = O) ≥ IAH > (−N-).The presence of ether bonds (−O-) and carboxyl groups (–COOH), which have high oxygen content, hinders CH_4 adsorption, aligning with Shi et al. [44]. The binding energy of O_2 at (–COOH), (−O-), and (–CH = O) exceeds the isosteric adsorption heat, suggesting that coal with high oxygen content facilitates O_2 adsorption and exothermic release. Typically, lower − rank coal contains more oxygen-functional groups, enhancing its selectivity for O_2 in CH_4/O_2 competitive adsorption, thereby increasing the risk of spontaneous combustion.

5. Conclusions

In this study, GCMC, MD, and DFT were employed to investigate the competitive adsorption behavior of CH_4/O_2 at varying temperatures, adsorption equilibrium pressures, and component ratios. The main conclusions are summarized as follows:

1) The competitive adsorption of the CH_4/O_2 binary gas mixture on coal exhibits distinct type I adsorption isotherm characteristics. Under identical temperature and pressure conditions, CH_4 exhibits a greater absolute adsorption amount compared to O_2. The overall adsorption of the mixed gas is largely unaffected by the component ratio. However, when the proportion of O_2 exceeds 78.5 %, the adsorption of O_2 surpasses that of CH_4. The adsorption isotherm fitting sequence is as follows: L-F model > Toth model > Langmuir model > Freundlich model.

2) The selectivity of coal for CH_4 over O_2 was found to decrease exponentially with increasing equilibrium pressure and linearly with rising temperature and CH_4 fraction. Higher pressure, temperature, and CH_4 concentration favor the competitive adsorption of O_2. At the critical ratio of CH_4:O_2 = 2.15:7.85, the competitive adsorption capacities of CH_4 and O_2 on the coal surface are equivalent, and this equilibrium remains unaffected by variations in pressure or temperature.

3) The ADF curve for the two gases shows a “double peak” skewed distribution. In competitive adsorption, CH_4 dominates the process and occupies the majority of sites in the strong adsorption zone. As the temperature rises from 273 K to 393 K, the initial adsorption energy of the CH_4/O_2 system first increases and then decreases. In multi-

component adsorption systems, the adsorption potential distribution is influenced by the gas mole fraction. As the CH_4 proportion increases from 0.2 to 0.8, the initial adsorption potential of CH_4 improves by 8.8 %, while the initial adsorption potential of O_2 decreases by 14.5 %.

4) The RDF curves for CH_4/O_2 relative to the main atoms on the coal surface show similar peak positions for C and H atoms. However, more distinct and significant peaks are observed for N and O atoms. The adsorption sites containing N and O are more specific, and since the CH_4 peak is greater than the O_2 peak, methane's competitive adsorption is dominant.

5) The binding energies of functional groups for CH_4 follow this order: (–CH = O) > (−N-) > IAH > (–COOH) > (−O-). For O_2, the binding energy sequence is: (–COOH) > (−O-) > (–CH = O) ≥ IAH > (−N-). Increased oxygen-containing functional groups enhance the competitive adsorption of O_2.

In summary, this study provides valuable insights for the prevention and control of CSC. However, the presence of moisture and metal salts in coal may influence the competitive adsorption of gases on the coal surface. Future research will focus on investigating the effects of coal moisture content and salt concentration on this process.

CRediT authorship contribution statement

Chengyang Peng: Writing – review & editing, Writing – original draft, Formal analysis, Data curation. **Shujing He:** Visualization, Funding acquisition. **Jianhong Kang:** Supervision, Conceptualization. **Ran Zhang:** Visualization, Methodology, Investigation. **Shasha Si:** Visualization, Project administration, Methodology. **Yiqian Zhou:** Validation, Software.

Declaration of competing interest

The authors declare that they have no known competing financial interests or personal relationships that could have appeared to influence the work reported in this paper.

Acknowledgements

This work was supported by the National Natural Science Foundation of China (Grant Nos. 52274240, 52227901), the Graduate Innovation Program of China University of Mining and Technology (Grant No. 2024WLKXJ163), and the Postgraduate Research & Practice Innovation Program of Jiangsu Province (Grant No. KYCX24_2934). Thanks to all the reviewers and editors for their work.

Data availability

Data will be made available on request.

References

[1] Ayawei N, Ebelegi AN, Wankasi D. Modelling and interpretation of adsorption Isotherms. J Chem 2017;2017:3039817. https://doi.org/10.1155/2017/3039817.
[2] Bai Z, Wang C, Deng J, Kang F, Shu C-M. Experimental investigation on using ionic liquid to control spontaneous combustion of lignite. Process Saf Environ Prot 2020; 142:138–49. https://doi.org/10.1016/j.psep.2020.06.017.
[3] Bonis LJ, Duga JJ. Fundamental phenomena in the materials sciences. Science 1967;155:357–61. https://doi.org/10.1126/science.155.3760.357.
[4] Carter MC, Kilduff JE, Weber WJ. Site energy distribution analysis of preloaded adsorbents. Environ Sci Technol 1995;29:1773–80. https://doi.org/10.1021/es00007a013.
[5] Chen F, Tang J, Wang J. Effects of π-π stacking on shale gas adsorption and transport in nanopores. ACS Omega 2023;8:46577–88. https://doi.org/10.1021/acsomega.3c05522.
[6] Dang Y, Zhao L, Lu X, Xu J, Sang P, Guo S, et al. Molecular simulation of CO_2/CH_4 adsorption in brown coal: effect of oxygen-, nitrogen-, and sulfur-containing functional groups. Appl Surf Sci 2017;423:33–42. https://doi.org/10.1016/j.apsusc.2017.06.143.
[7] Deng J, Ren S-J, Xiao Y, Li Q-W, Shu C-M, Bai G-Y. Thermophysical properties of coal during low temperature oxidation under different oxygen concentrations. Thermochim Acta 2019;676:186–97. https://doi.org/10.1016/j.tca.2019.05.003.
[8] Deng J-H, Luo J, Mao Y-L, Lai S, Gong Y-N, Zhong D-C, et al. π-π stacking interactions: Non-negligible forces for stabilizing porous supramolecular frameworks. Sci Adv 2020;6:eaax9976. https://doi.org/10.1126/sciadv.aax9976.
[9] Do DD, Nicholson D, Do HD. On the Henry constant and isosteric heat at zero loading in gas phase adsorption. J Colloid Interface Sci 2008;324:15–24. https://doi.org/10.1016/j.jcis.2008.05.028.
[10] Düzgün HS, Leveson N. Analysis of soma mine disaster using causal analysis based on systems theory (CAST). Saf Sci 2018;110:37–57. https://doi.org/10.1016/j.ssci.2018.07.028.
[11] Freundlich H. Over the adsorption in solution. J Phys Chem 1906;57(385471): 1100–7.
[12] Fu S, Wang L, Li S, Ni S, Cheng Y, Zhang X, et al. Re-thinking methane storage mechanism in highly metamorphic coalbed reservoirs — a molecular simulation considering organic components. Energy 2024;293:130444. https://doi.org/10.1016/j.energy.2024.130444.
[13] Hao M, Wei C, Nie Y. Influence of combustible gases from coal spontaneous combustion on CH_4 adsorption in the goaf. Chem Phys Lett 2022;803:139806. https://doi.org/10.1016/j.cplett.2022.139806.
[14] Kang J, Zhou F, Xia T, Ye G. Numerical modeling and experimental validation of anomalous time and space subdiffusion for gas transport in porous coal matrix. Int J Heat Mass Transf 2016;100:747–57. https://doi.org/10.1016/j.ijheatmasstransfer.2016.04.110.
[15] Kim HJ, Shi Y, He J, Lee H-H, Lee C-H. Adsorption characteristics of CO_2 and CH_4 on dry and wet coal from subcritical to supercritical conditions. Chem Eng J 2011; 171:45–53. https://doi.org/10.1016/j.cej.2011.03.035.
[16] Koble RA, Corrigan TE. Adsorption isotherms for pure hydrocarbons. Ind Eng Chem 1952;44:383–7. https://doi.org/10.1021/ie50506a049.
[17] Kumar KV, Gadipelli S, Wood B, Ramisetty KA, Stewart AA, Howard CA, et al. Characterization of the adsorption site energies and heterogeneous surfaces of porous materials. J Mater Chem A 2019;7:10104–37. https://doi.org/10.1039/c9ta00287a.
[18] Langmuir I. The adsorption of gases on plane surfaces of glass, mica and platinum. J Am Chem Soc 1918;40:1361–403. https://doi.org/10.1021/ja02242a004.
[19] Li L, Fan H, Hu H. Distribution of hydroxyl group in coal structure: a theoretical investigation. Fuel 2017;189:195–202. https://doi.org/10.1016/j.fuel.2016.10.091.
[20] Li Z, Ren T, Li X, Cheng Y, He X, Lin J, et al. Full-scale pore structure characterization of different rank coals and its impact on gas adsorption capacity: a theoretical model and experimental study. Energy 2023;277:127621. https://doi.org/10.1016/j.energy.2023.127621.
[21] Liu H, Li Z, Yang Y, Miao G, Li J. The temperature rise characteristics of coal during the spontaneous combustion latency. Fuel 2022;326:125086. https://doi.org/10.1016/j.fuel.2022.125086.
[22] Liu Y, Wen H, Guo J, Jin Y, Wei G, Yang Z. Coal spontaneous combustion and N_2 suppression in triple goafs: a numerical simulation and experimental study. Fuel 2020;271:117625. https://doi.org/10.1016/j.fuel.2020.117625.
[23] Long, H., Lin, H., Yan, M., Chang, P., Li, S. gang, Bai, Y., 2021. Molecular simulation of the competitive adsorption characteristics of CH_4, CO_2, N_2, and multicomponent gases in coal. Powder Technology 385, 348–356. https://doi.org/10.1016/j.powtec.2021.03.007.
[24] Ma D, Qin B, Zhong X, Sheng P, Yin C. Effect of flammable gases produced from spontaneous smoldering combustion of coal on methane explosion in coal mines. Energy 2023;279:128125. https://doi.org/10.1016/j.energy.2023.128125.
[25] Ma Z, Qin B, Shi Q, Zhu T, Chen X, Liu H. The location analysis and efficient control of hidden coal spontaneous combustion disaster in coal mine goaf: a case study. Process Saf Environ Prot 2024;184:66–78. https://doi.org/10.1016/j.psep.2024.01.054.
[26] Meng J, Li S, Niu J, Meng H, Zhong R, Zhang L, et al. Effects of moisture on methane desorption characteristics of the Zhaozhuang coal: experiment and molecular simulation. Environ Earth Sci 2020;79:44. https://doi.org/10.1007/s12665-019-8788-9.
[27] Meng J, Zhong R, Li S, Yin F, Nie B. Molecular model construction and study of gas adsorption of Zhaozhuang coal. Energy Fuels 2018;32:9727–37. https://doi.org/10.1021/acs.energyfuels.8b01940.
[28] Onifade M, Genc B. A review of research on spontaneous combustion of coal. Int J Min Sci Technol 2020;30:303–11. https://doi.org/10.1016/j.ijmst.2020.03.001.
[29] Onifade M, Genc B. A review of spontaneous combustion studies – South African context. Int J Min Reclam Environ 2019;33:527–47. https://doi.org/10.1080/17480930.2018.1466402.
[30] Qin B, Li L, Ma D, Lu Y, Zhong X, Jia Y. Control technology for the avoidance of the simultaneous occurrence of a methane explosion and spontaneous coal combustion in a coal mine: a case study. Process Saf Environ Protect 2016;103:203–11. https://doi.org/10.1016/j.psep.2016.07.005.
[31] Shi T, Wang XF, Deng J, Wen ZY. The mechanism at the initial stage of the room-temperature oxidation of coal. Combust Flame 2005;140:332–45. https://doi.org/10.1016/j.combustflame.2004.10.012.
[32] Stracher, G.B., Taylor, T.P., 2004. Coal fires burning out of control around the world: thermodynamic recipe for environmental catastrophe. International Journal of Coal Geology, Coal Fires Burning around the World: a Global Catastrophe 59, 7–17. https://doi.org/10.1016/j.coal.2003.03.002.
[33] Toth. 1971. State equations of the solid gas interface layer. Acta Chem. Acad. Hung., 69, 311-317.

[34] Voigt, S., Tetzlaff, A., Zhang, J., Künzer, C., Zhukov, B., Strunz, G., Oertel, D., Roth, A., van Dijk, P., Mehl, H., 2004. Integrating satellite remote sensing techniques for detection and analysis of uncontrolled coal seam fires in North China. International Journal of Coal Geology, Coal Fires Burning around the World: a Global Catastrophe 59, 121–136. https://doi.org/10.1016/j.coal.2003.12.013.

[35] Wang HH, Dlugogorski BZ, Kennedy EM. Coal oxidation at low temperatures: oxygen consumption, oxidation products, reaction mechanism and kinetic modelling. Prog Energy Combust Sci 2003;29:487–513. https://doi.org/10.1016/S0360-1285(03)00042-X.

[36] Wu C, Li J, Zhou F, Shi B. Experimental study on the competitive adsorption characteristics of N_2, CO_2 and O_2 with various CO_2/N_2 blend ratios in coal. Int J Hydrogen Energy 2024;59:924–36. https://doi.org/10.1016/j.ijhydene.2024.02.085.

[37] Xiang J, Zeng F, Liang H, Li B, Song X. Molecular simulation of the $CH_4/CO_2/H_2O$ adsorption onto the molecular structure of coal. Sci China-Earth Sci 2014;57:1749–59. https://doi.org/10.1007/s11430-014-4849-9.

[38] Yan L, Wen H, Liu W, Jin Y, Liu Y, Li C. Adiabatic spontaneous coal combustion period derived from the thermal effect of spontaneous combustion. Energy 2022;239:122101. https://doi.org/10.1016/j.energy.2021.122101.

[39] Yu S, Bo J, Fengjuan L. Competitive adsorption of $CO_2/N_2/CH_4$ onto coal vitrinite macromolecular: effects of electrostatic interactions and oxygen functionalities. Fuel 2019;235:23–38. https://doi.org/10.1016/j.fuel.2018.07.087.

[40] Zhang Y, Zhang Y, Li Y, Li Q, Zhang J, Yang C. Study on the characteristics of coal spontaneous combustion during the development and decaying processes. Process Saf Environ Protect 2020;138:9–17. https://doi.org/10.1016/j.psep.2020.02.038.

[41] Zhao J, Deng J, Chen L, Wang T, Song J, Zhang Y, et al. Correlation analysis of the functional groups and exothermic characteristics of bituminous coal molecules during high-temperature oxidation. Energy 2019;181:136–47. https://doi.org/10.1016/j.energy.2019.05.158.

[42] Zhang D, Yang X, Deng J, Wen H, Xiao Y, Jia H. Research on coal spontaneous combustion period based on pure oxygen adiabatic oxidation experiment. Fuel 2021;288:119651. https://doi.org/10.1016/j.fuel.2020.119651.

[43] Li P, Ma D, Zhang H, Li W, Yang F. Influence of high and low rank coal wettability and methane adsorption/desorption characteristics. Coal Geol Explor 2016;44:80–5. https://doi.org/10.3969/j.issn.1001-1986.2016.05.015.

[44] Shi Y, Yang X, Xue J, Li S, Yang M, Liu Y. Analysis of effects of microstructure of tectonically-deformed coal on the CO_2 and CH_4 competitive adsorption capacity. Mining Saf Environ Prot 2022;49:34–42. https://doi.org/10.19835/j.issn.1008-4495.2022.05.007.

[45] Cheng Y, Hu B. Main occurrence form of methane in coal: Micropore filling. J China Coal Soc 2021;46:2933–48. https://doi.org/10.13225/j.cnki.jccs.2020.1214.

[46] Nie B, Duan S. The adsorption essence of gas on coal surface. J Taiyuan Univ Technol 1998:88–92. https://doi.org/10.16355/j.cnki.issn1007-9432tyut.1998.04.027.